

# PCCP

Accepted Manuscript



This is an *Accepted Manuscript*, which has been through the Royal Society of Chemistry peer review process and has been accepted for publication.

*Accepted Manuscripts* are published online shortly after acceptance, before technical editing, formatting and proof reading. Using this free service, authors can make their results available to the community, in citable form, before we publish the edited article. We will replace this *Accepted Manuscript* with the edited and formatted *Advance Article* as soon as it is available.

You can find more information about *Accepted Manuscripts* in the [Information for Authors](#).

Please note that technical editing may introduce minor changes to the text and/or graphics, which may alter content. The journal's standard [Terms & Conditions](#) and the [Ethical guidelines](#) still apply. In no event shall the Royal Society of Chemistry be held responsible for any errors or omissions in this *Accepted Manuscript* or any consequences arising from the use of any information it contains.

# Atomic Under-coordination Induced Catalytic and Magnetic Fascinations of Pt and Rh nanoclusters

Cite this: DOI: 10.1039/x0xx00000x

Shideh Ahmadi,<sup>a</sup> Xi Zhang,<sup>a</sup> Yinyan Gong<sup>b</sup> and Chang Q. Sun<sup>a</sup>

Received 00th January 2012,  
Accepted 00th January 2012

DOI: 10.1039/x0xx00000x

www.rsc.org/

Density functional theory (DFT) calculations with local spin density discrimination have been performed to exam the effect of atomic under-coordination on the catalytic and magnetic properties of Cuboctahedral (CO) and Marks Decahedral (MD) structured Pt and Rh nanoclusters. Consistency between theoretical calculations and experimental observations confirmed the predictions based on the framework of bond-order-length-strength (BOLS) correlation and nonbonding electron polarization (NEP) notations. The BOLS-NEP notation suggests that the shorter-and-stronger bonds between under-coordinated atoms induce local densification and quantum entrapment of core electrons, which then polarize the otherwise conducting electrons and result in shifts of the binding energy. Such strong localization resolves the intriguing catalytic and magnetic attributes of Pt and Rh nanoclusters.

## Introduction

Metallic nanoparticles (NPs) have attracted enormous interest due to their intriguing chemical and physical properties which cannot be observed in their bulk counterparts.<sup>1</sup> A key difference between a nanosolid and its bulk counterpart is the high fraction of under-coordinated atoms in the skin consisting of a few atomic layers. As the size of a NP decreases, the volume ratio of the surface layers to the entire body, referred to as the surface-to-volume ratio, increases dramatically. For instance, as the diameter of a spherical dot decreases from 1  $\mu\text{m}$  to 10 nm, the surface-to-volume ratio increases from 1% to 25%. The interaction between the under-coordinated atoms at the skin modifies the electronic structure and distinguishes NPs from their bulk counterparts in performance because of the bond contraction and bond energy elevation induced by atomic under-coordination.<sup>1</sup> For example, Rh NPs exhibit giant magnetic moments<sup>2, 3</sup> though the bulk Rh is diamagnetic. Similarly, Pt also transforms from non-magnetic to magnetic as the size is reduced from bulk to a few nanometers.<sup>2, 4</sup> The giant magnetic moments observed in these metallic NPs make them potential candidates for nanospintronic applications<sup>5</sup> and magnetic data storage.<sup>6</sup> Moreover, the catalytic ability of Au, Pt, Pd, and Rh NPs are greatly enhanced;<sup>7</sup> and a phase transition from conductor to insulator happens at the nanometer scale.<sup>8, 9</sup>

At the nanometer scale, the potential trap depth, charge density, energy density, as well as electronic configurations of

metallic NPs differ from their bulk counterparts, accompanying the structure evolution from face-centred-cubic to icosahedral<sup>10, 11</sup> or decahedral,<sup>12, 13</sup> as well as surface bond contraction. X-ray photoelectron spectroscopy (XPS) measurements have revealed positive core-level shifts (CLS) for Pt nanoclusters deposited on pristine carbon nanotubes (CNTs)<sup>14, 15</sup> and highly oriented pyrolytic graphite (HOPG).<sup>16</sup> Moreover, the peaks of valence local-density-of-states (LDOS) of Ag nanoclusters,<sup>17</sup> Rh NPs,<sup>18</sup> Au atomic chain,<sup>19</sup> Au nanowires,<sup>20</sup> Cu monatomic chain,<sup>21</sup> and Pt nanoclusters<sup>22</sup> are all shifted to upper energies as observed by scanning tunnelling microscope/spectroscopy (STM/S). Although atoms forming nanoclusters or located at the edges or at the chain ends demonstrate so many fascinating properties, the mechanism behind them remains yet unclear, and thus a thorough understanding of the under-coordination effects of Pt and Rh nanoclusters on their properties is highly desirable.

In recent decades, *ab initio* density functional theory (DFT) calculation has become an elegant tool to investigate the properties of various materials. With the simplification of inserting a vacuum slab into the periodic structure or by neglecting the edge potentials or edge states, DFT calculations can be applied to non-periodic system. For instance, DFT calculations have been applied successfully to study the enhanced electrocatalytic activity of mushroom-like Pt clusters on Pd-shell over Au core NPs,<sup>23</sup> as well as the isotope shifts in Pt and Rh NMR spectra.<sup>24</sup> Previously, we have successfully applied this method to study the electronic properties of Au,<sup>25</sup>

Ag,<sup>26</sup> and Cu<sup>26</sup> nanoclusters. Here, we report consistency in trend between DFT calculations and the experimental observations on the local bond contraction, charge transfer, lattice strain, CLS, valence electron polarization, as well as magnetization of Pt and Rh nanoclusters. This agreement confirms our expectations based on the framework of the bond-order-length-strength (BOLS) correlation and nonbonding electron polarization (NEP) premise, which stressed that the atomic under-coordination induces the unusual catalytic and magnetic properties of metal nanoclusters.

## Principles and approaches

**Tight-binding approximation.** According to the band theory, the  $v$ th energy level of an isolated atom,  $E_v(0)$ , is determined by integrating the intra-atomic potential,  $V_{atom}(r)$ , and the eigenfunction of an atom at a specific  $i$ th atomic site,  $|v, i\rangle$ . Due to the involvement of the inter-atomic potential,  $V_{cryst}(r)$ , the core-level binding energy shifts from  $E_v(0)$  to  $E_v(K)$  by an amount proportional to the cohesive energy per bond at equilibrium,<sup>27</sup>

$$H = -\frac{\hbar^2 \nabla^2}{2m} + V_{atom}(r) + V_{cryst}(r)$$

$$E_v(0) = \langle v, i | V_{atom}(r) | v, i \rangle \quad (\text{Core level energy})$$

$$\Delta E_v(K) = E_v(K) - E_v(0) = \langle v, i | V_{cryst}(r) | v, i \rangle + \sum_{j=1}^{z-1} \langle v, i | V_{cryst}(r) | v, j \rangle$$

$$= \beta + z\gamma \propto \langle E_b \rangle \quad (\text{Core level shift}) \quad (1)$$

$$\begin{cases} \beta = \langle v, i | V_{cryst}(r) | v, i \rangle \propto \langle E_b \rangle & (\text{Exchange integral}) \\ \gamma = \langle v, i | V_{cryst}(r) | v, j \rangle \propto \langle E_b \rangle & (\text{Overlap integral}) \end{cases} \quad (2)$$

The coordination numbers  $z = 0$  and  $K$  represents an isolated atom and an atom in the bulk, respectively. The sum is over all  $z$  neighbours of the specific  $i$ th atom. The exchange and overlap integrals are relative to the cohesive energy per bond  $\langle E_b \rangle$ . Because  $\langle v, i | v, j \rangle = \delta_{ij}$  with  $\delta_{ij}$  being the Kronecker function (if  $i = j$ ,  $\delta_{ij} = 1$ , otherwise,  $\delta_{ij} = 0$ ), the term  $z\gamma/\beta \ll 1$ . Any perturbation to the bond energy  $E_b$  will shift the core level accordingly.

## BOLS-NEP correlation: Quantum entrapment, lattice contraction, and polarization

**BOLS correlation.** Extended from the ‘‘atomic coordination-atomic radius’’ correlation premise of Goldschmit<sup>28</sup> and Pauling,<sup>29</sup> the BOLS correlation theory<sup>1</sup> deals with under-coordinated systems such as adatoms, defects, surfaces, and nanoclusters. According to the BOLS theory, the shorter and stronger bonds between the under-coordinated atoms cause local densification and quantum entrapment of binding energy and core electrons, which then polarize of the otherwise conductive charges and make the nanocrystals nonconductive and magnetic. The extent of entrapment and polarization

increases with the reduction of atomic coordination number (CN). The BOLS correlation can be expressed by:

$$\begin{cases} z_i = 4(1 - 0.75/K); z_2 = z_1 + 2; z_3 = 12 & (\text{Effective Coordination}) \\ d_i = C_i d_b = 2d_b / [1 + \exp((12 - z_i)/8z_i)] & (\text{Bond Contraction Coefficient}) \\ E_i = C_i^m E_b & (\text{Bond Energy : Potential Trap}) \end{cases} \quad (3)$$

where subscripts  $i$  and  $b$  denote atoms in the  $i$ th atomic layer counted from the outermost to the centre of a sphere and in the bulk, respectively;  $K = R/d$  is the number of atoms lined along the radius of a spherical dot or across the thickness of a plate;  $d_i$  and  $E_i$  are the bond length and single bond energy between under-coordinated atoms, respectively;  $m$  is the bond nature index, correlating the bond energy with the bond length, and is extracted by fitting experimental data with BOLS premise.<sup>1</sup> Eqn (3) indicates that for the under-coordinated atoms at the  $i$ th shell of NPs, the bond binding energy will increase as the bonds contract.

According to the energy band theory under tight-binding (TB) approximation<sup>27</sup> and the BOLS correlation,<sup>1</sup> the Hamiltonian of a nanocrystal undertakes the perturbation ( $\Delta_H$ ) because of the atomic CN deficiency in the skin while the intra-atomic trapping remains invariable:<sup>30</sup>

$$V(\Delta_i) = V_{atom}(r) + V_{cryst}(r)[1 + \Delta_H]$$

where

$$\Delta_H = \begin{cases} \sum_{i=3}^{\infty} \gamma_i (C_i^m - 1) = \tau K^{-1} \sum_{i=3}^{\infty} C_i (C_i^m - 1) = \Delta'_H \tau K^{-1} & (\text{Nanostructure}) \\ C_i^m - 1 & (\text{Surface}) \end{cases} \quad (4)$$

where  $\gamma_i = \tau C_i K^{-1}$  is the surface-to-volume ratio,  $i$  counts from the outermost layer inwards up to three, and  $\tau = 1, 2$ , and  $3$  is the geometric shape factor for a thin plate, a cylindrical rod, and a spherical dot, respectively. From the electronic structure point of view, the surface constitutes at most three atomic layers or two inter-atomic spacing since only the under-coordinated atoms in the skin induce perturbation  $\Delta_H$  to the overall Hamiltonian. The  $\Delta_H$  ( $\tau, K, K^{-1}, m, z_i, d_i, E_i$ ) includes all the possible extrinsic contributions from the curvature, shape, size, as well as the intrinsic contributions from bond nature, length, order, and energy to the Hamiltonian.

**Lattice contraction.** Due to the surface bond contraction, the mean lattice constants of the entire nanosolid will be reduced, and the mean surface strain can be expressed by:

$$\begin{cases} \bar{d} = d_b [1 + \Delta_d] \\ \frac{\Delta d}{d} = \Delta_d = \sum_{i=3}^{\infty} \gamma_i (C_i - 1) = \tau K^{-1} \sum_{i=3}^{\infty} C_i (C_i - 1) = \Delta'_d \tau K^{-1} \end{cases} \quad (5)$$

It is found that the relative change in the mean lattice constant of a nanosolid simply depends on its shape, size, as well as the bond contraction coefficient.

**Energy entrapment.** By incorporating the BOLS correlation into the band theory, one can obtain the energy shift of an atom

at a specific  $\nu$ th energy level in the skin relative to an isolated atom:<sup>1</sup>

$$\begin{cases} \Delta E_{\nu}(K) = E_{\nu}(K) - E_{\nu}(0) = \Delta E_{\nu}(\infty)(1 + \Delta_H) = [E_{\nu}(\infty) - E_{\nu}(0)](1 + \Delta_H) \\ \frac{E_{\nu}(K) - E_{\nu}(0)}{E_{\nu}(\infty) - E_{\nu}(0)} = 1 + \Delta_H \end{cases} \quad (6)$$

where  $E_{\nu}(0)$  is the core-level position of an isolated atom,  $\Delta E_{\nu}(K)$  is the atomic under-coordination induced CLS,  $E_{\nu}(K)$  is the XPS peak of the  $\nu$ th band, and  $E_{\nu}(\infty)$  is the bulk counterpart. Hence, one is able to determine  $E_{\nu}(0)$  and  $\Delta E_{\nu}(\infty)$  from XPS spectra measurements. Generally, the size-induced binding energy shift of nanostructures is inversely proportional to its size  $K$ , in the form of  $E_{\nu}(K) = A + CK^{-1}$ , where constants  $A$  and  $C$  can be extracted from the measured  $E_{\nu}(K)$  vs. size using the least-root-mean-square linearization method. By equalling the experimental scaling correlation with the theoretical illustration, the following expression is obtained from Eqn (6):

$$E_{\nu}(K) = \begin{cases} E_{\nu}(\infty) + [E_{\nu}(\infty) - E_{\nu}(0)]\tau\Delta'_H K^{-1} & \text{(BOLS theory)} \\ A + CK^{-1} & \text{(Measurement)} \end{cases} \quad (7)$$

By equalling the theoretical formulation to the experimental measurements, the following expression can be obtained:

$$\begin{cases} A = E_{\nu}(\infty) \\ C = [E_{\nu}(\infty) - E_{\nu}(0)]\tau\Delta'_H \end{cases} \quad (8)$$

Therefore, the  $\nu$ th energy level of an isolated atom and its bulk shift can be expressed by

$$\begin{cases} E_{\nu}(0) = A - \frac{C}{\tau\Delta'_H} & \text{(Atomic energy level)} \\ \Delta E_{\nu}(\infty) = \frac{C}{\tau\Delta'_H} & \text{(Bulk shift)} \end{cases} \quad (9)$$

**DFT calculations.** In order to verify the predications based on the BOLS correlation such as quantum entrapment and the associated charge polarization, we conducted DFT calculations on the bond relaxation, charge transfer, valence polarization, magnetic momentum, and magnetization of Pt and Rh nanoclusters, and compared the calculated results with experimental observations including the extended X-ray absorption fine structure (EXAFS), STM/S, X-ray photoelectron differential spectroscopy (XPDS), and XPS.

Many theoretical and experimental efforts have been devoted to determine the structures of Pt and Rh nanoclusters.<sup>12, 31-34</sup> It is generally accepted that icosahedral<sup>10, 35</sup> or decahedral<sup>12, 13</sup> structures are stable structures of transitional metal NPs such as Pt and Rh NPs. For instance, Marks Decahedral (MD) structures have been observed experimentally in Pt NPs prepared by gas evaporation,<sup>13</sup> and Rh NPs epitaxial deposited on NaCl(001).<sup>36</sup> However, some research groups

claimed that fcc-like Cuboctahedral (CO) structures are stable form for Pt nanocrystals prepared by electrocatalytic hydrogenation<sup>32</sup> and Rh nanocrystals grown on NaCl substrates.<sup>31</sup> Previous DFT calculations also showed that the structures of multiply-twinned Pt<sup>37</sup> and Rh<sup>38</sup> clusters are CO. Hence, we adopted both CO structures (13, 55, and 147 atoms) and MD structures (13, 49, and 57 atoms) in our calculations of Pt and Rh nanoclusters (see Fig. 1).

The DFT calculations were carried out using the DMol<sup>3</sup> code with a double numeric plus polarization (DNP) basis set.<sup>39, 40</sup> During the DFT calculations, the potentials of core electrons are assumed to be semi-core pseudopotential.<sup>41</sup> The DFT exchange-correlation potential utilized the local spin density approximation (LSDA), with the PWC function for geometry and electronic structures.<sup>42</sup> To demonstrate the under-coordinated effects on the properties of NPs, we considered the singlet and triplet ground states for Pt nanoclusters and quartet ground state for Rh nanoclusters. To achieve self-consistent-field (SCF) convergence, thermal occupation was used instead of the Fermi for open-shell system with unrestricted wavefunction. In spin-unrestricted wavefunction, different orbitals are related to different spins including spin-up ( $\alpha$ ) and spin-down ( $\beta$ ). The self-consistency threshold of total energy was set at  $10^{-6}$  Hartree in the calculations. The tolerance energy, forces, and displacement in the geometry optimization were taken as  $10^{-5}$  Hartree, 0.002 Hartree/Å, and 0.005Å, respectively.

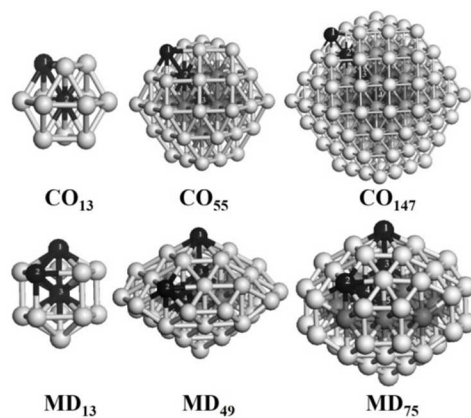


**Fig. 1.** The CO and MD geometric structures of Pt<sub>N</sub> and Rh<sub>N</sub> nanoclusters consisted of 13-147 atoms. The numbers denote positions of atoms at different shells.

## Results and discussion

**Skin-resolved bond length contraction.** The results of DFT calculations are listed in Table 1. As expected, spontaneous bond contraction at the surface of Pt and Rh nanoclusters is observed and the extent of bond contraction depends only on the atomic CN. For instance, the calculated Pt-Pt distance of Pt nanoclusters in the outermost shell of CO<sub>147</sub> is 2.663 Å and 2.685 Å for singlet and triplet states, respectively, which are significantly smaller than the bulk value of 2.770 Å.<sup>43</sup> Similar trends are observed for other CO structures and all the MD

structures of various sizes. Results obtained here by combing BOLS correlation and DFT calculations are in good agreement with the previous results.<sup>4, 43-47</sup> For example, Sang et al.<sup>46</sup> showed by DFT calculations that the Pt-Pt distance is decreased to 2.400 Å and 2.580 Å for dimer and trimer, respectively. Up to 10-15%<sup>44</sup> and 13%<sup>47</sup> bond contraction for Pt dimer are also revealed by DFT calculations and molecular dynamic calculations, respectively. In addition, the bond contraction of Pt clusters<sup>4</sup> and monoatomic chains<sup>43</sup> is observed experimentally. For Rh nanoclusters, the calculated bond length of the outmost shell of CO<sub>147</sub> is about 2.685 Å, exhibiting a clear reduction compared to the bulk value of 2.690 Å.<sup>48</sup> The observed trend of bond contraction at the surface is consistent with the previous report. For instance, bond contraction up to 14%,<sup>49</sup> 4%,<sup>48</sup> and 4-8%,<sup>49</sup> are observed by local-spin-density-functional model and TB approximation for Rh dimer, Rh<sub>13</sub> clusters, and larger Rh clusters, respectively. In addition, Villaseñor-González et al.<sup>50</sup> and Barreateau et al.<sup>51</sup> reported about 2 to 9% bond contraction for Rh clusters and 3-5% bond contraction for Rh clusters with 13, 55, 147, 309, and 561 atoms based on TB approximation.

We note that the bond lengths of the outermost shells, with smaller curvature-dependent CN shrink more than those of the interior (see Table 1). For instance, for the singlet states of the Pt CO<sub>147</sub> nanoclusters, the calculated Pt-Pt distance decreases from 2.763 Å to 2.663 Å in the direction from the interior toward the outermost shells as the effective CN decreases from 12 to 3.14. For nanoclusters with different sizes, the bond length varies in a similar way except for atoms with comparable CN. It is important to point out that the DFT calculations tend to underestimate bond contraction compared with the expectation based on BOLS correlation. However, the origin for this quantitative deviation is still unclear and need a systemic study in the future.

**Lattice strain.** The lattice strain estimated based on BOLS correlation (solid line) and the measured size-dependent mean lattice contraction (scattered data) are plotted in Fig. 2. The intercepts and slopes in the scaling law were extracted by linearizing the experimental data with the least-root-mean-square optimization method. According to Eqn (5), the mean lattice strain of Pt and Rh NPs is inversely proportional to the size of Pt and Rh NPs. Our calculations include experimental results on Pt deposition on NiAl (110) substrate,<sup>52</sup> Pt on Cu(111) surface at 300K,<sup>53</sup> Pt(422) surface, Pt(111) surface<sup>54</sup> and Rh surface.<sup>55</sup> It shows consistently that the lattice contraction is a function of NPs size, and confirms that the bond-order loss and CNs imperfection affect lattice strain.

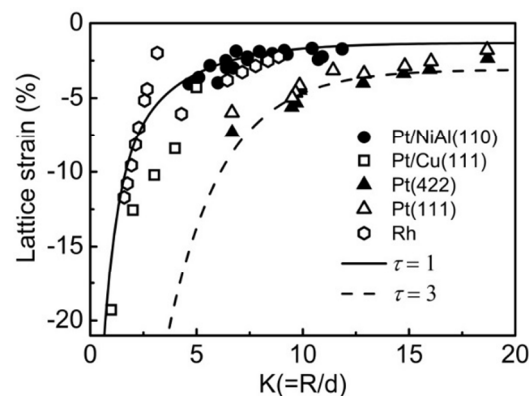


**Fig.2.** Consistency in trend between theoretical predictions (solid line) and various experimental observations (scattered data) of the mean lattice contraction of Pt and Rh NPs including Pt deposited on NiAl(110) substrate,<sup>52</sup> on Cu (111) at 300K,<sup>53</sup> on Pt (422) and Pt (111) at 300K,<sup>54</sup> as well as Rh.<sup>55</sup> In our calculations,  $\tau = 1$  and 3 for a plate and a sphere dot, respectively,  $z_1 = 4$  and  $z_2 = 6$ , and  $K$  is dimensionless.

**Table 1.** The effective CN ( $z_i$ ), bond length ( $d_i$ ), bond contraction coefficient ( $C_i$ ), shell index ( $i$ ), magnetic moment ( $\mu$ ), and “charge transfer” of atoms at different positions of Pt<sub>N</sub> and Rh<sub>N</sub> nanoclusters

Structure	Position atom	$z_i$	$d_i$ (Å)			$C_i-1$ (%)		Shell $i$	Magnetic moment ( $\mu$ )		“Charge Transfer” ( $e$ )		
			Pt	Pt	Rh	Pt	Rh		Pt	Rh	Pt	Pt	Rh
CO <sub>13</sub>	1~2	2.00	Singlet	Triplet									
			Pt	Pt	Rh	Pt	Rh	Pt	Rh	Pt	Pt	Rh	
CO <sub>55</sub>	1~2	2.80											
			Pt	Pt	Rh	Pt	Rh	Pt	Rh	Pt	Pt	Rh	
CO <sub>147</sub>	2~3	4.80											
			Pt	Pt	Rh	Pt	Rh	Pt	Rh	Pt	Pt	Rh	
MD <sub>13</sub>	1~2	3.14											
			Pt	Pt	Rh	Pt	Rh	Pt	Rh	Pt	Pt	Rh	
			Pt	Pt	Rh	Pt	Rh	Pt	Rh	Pt	Pt	Rh	
MD <sub>49</sub>	2~3	5.14											
			Pt	Pt	Rh	Pt	Rh	Pt	Rh	Pt	Pt	Rh	
			Pt	Pt	Rh	Pt	Rh	Pt	Rh	Pt	Pt	Rh	
MD <sub>75</sub>	3~4	12.00											
			Pt	Pt	Rh	Pt	Rh	Pt	Rh	Pt	Pt	Rh	
			Pt	Pt	Rh	Pt	Rh	Pt	Rh	Pt	Pt	Rh	

**Potential trap depression and “charge transfer” from centre to edge.** According to the principle of the least energy, any spontaneous process proceeds toward the direction of energy reduction. Therefore, the spontaneous process of bond contraction is associated with the inter-atomic potential well depression or the bond energy gain, and electrons have a higher density at the surface than in the core, referred to as “charge transfer” from the interior shell to the outermost shell. Energetically, the core-level binding energy will go deeper, referred to as positive CLS,<sup>56</sup> and the extent is determined uniquely by the overlap and exchange integrals, or the coupling of the inter-atomic potential and the specific Bloch wave functions. Therefore, the charges will be localized at the surface due to the surface potential depression and the core electron energy level deepening, which in turn polarize the loosely bond valence electrons.

The “charge transfer” of CO (13, 55, and 147 atoms) and MD (13, 49, and 75 atoms) structures for Pt and Rh nanoclusters was estimated using Mulliken population analysis,<sup>57</sup> and the results are listed in Table 1. The negative and positive signs in Table 1 represent charge gain and charge loss, respectively. It can be seen that the outermost shells gain excessive charges whereas the interior shells loss. For example, the calculated value of “charge transfer” for Pt CO<sub>147</sub> (triplet state) changes from -0.681  $e$  in the outermost shell to 0.254  $e$  in the interior shell, indicating that the electrons have a higher density at the surface of the nanoclusters. This is consistent with the previous work on Au (111) nanoclusters,<sup>58</sup> Cu-Ag clusters,<sup>59</sup> Au-Ag clusters,<sup>60</sup> Au nanoclusters,<sup>25</sup> as well as Ag and Cu nanoclusters.<sup>26</sup> To exam the stability of our calculations, Mulliken charge transfer is also calculated for CO<sub>13</sub> and MD<sub>13</sub> structures of Pt and Rh nanoclusters with smaller basis set (e.g double numerical (DN)<sup>39</sup>), and the obtained results are in good agreement with the values listed in Table 1 (see Table S1 and Figures S6-S9 in supplementary information).

**Core electron entrapment.** According to BOLS correlation, the core-level binding energy of under-coordinated atoms shifts toward deeper energies. Previously, a positive binding energy shift of about 0.6 eV, 0.5 eV and 0.65 eV has been reported for Pt NPs on pristine CNTs,<sup>14, 15</sup> and HOPG,<sup>16</sup> as well as Rh(110) surface,<sup>61</sup> respectively. Moreover, the deepening of the Pt 4f<sub>7/2</sub><sup>62</sup> and Rh 3d<sub>5/2</sub><sup>63</sup> core-level binding energy is also confirmed by high energy resolution core level photoelectron spectroscopy and DFT calculations.

**Table 2.** BOLS derived  $E_v(0)$  and  $\Delta E_v(\infty)$  for Pt<sub>N</sub> and Rh<sub>N</sub> nanoclusters. A and C are the intercept and slope of the linearization of the measured XPS data. The effective CN of  $z_1=4$ ,  $z_2=6$ , and  $z_3=12$  are considered during the calculation.

	A (eV)	C (eV)	$E_v(0)$ (eV)	$\Delta E_v(\infty)$ (eV)
Pt- Pristine CNTs <sup>64</sup>	71.26	0.66	67.21	4.05
Pt-HOPG <sup>14</sup>	71.15	0.58	67.21	3.94
Pt-TiO <sub>2</sub> (110)-300K <sup>65</sup>	71.11	0.70	67.21	3.90
Pt-MCNTs-untreated <sup>15</sup>	71.11	0.42	67.21	3.90
Pt-MCNTs-Ar <sup>+15</sup>	71.19	0.88	67.21	3.98
Pt-MCNTs-O <sub>2</sub> <sup>15</sup>	71.26	0.63	67.21	4.05
Rh-TiO <sub>2</sub> (110)-(1x1)-well ordered <sup>66</sup>	306.70	0.09	302.16	4.54
Rh-TiO <sub>2</sub> (110)-(1x1)-Slightly-Ar <sup>+66</sup>	306.70	0.12	302.16	4.54
Rh-TiO <sub>2</sub> (110)-(1x1)-Strongly- Ar <sup>+66</sup>	306.40	0.11	302.16	4.24
Rh-TiO <sub>2</sub> <sup>67</sup>	307.50	0.13	302.16	5.34
Rh-TiO <sub>2</sub> -300K <sup>68</sup>	307.30	0.08	302.16	5.14
Rh-TiO <sub>2</sub> -160K <sup>68</sup>	307.40	0.05	302.16	5.24

Table 2 listed the calculated  $E_v(0)$  and  $\Delta E_v(\infty)$  values for Pt-4f and Rh-3d based on Eqn (6) using results of XPS measurements reported in the cited references. Fig. 3 (a) and (b) plotted the

BOLS reproduction (solid line) of the measured shape- and size-dependence of the Pt-4*f* and Rh-3*d* CLS (scattered data). The intercepts and slopes in the scaling law are obtained by linearizing the experimental data with the least-root-mean-square optimization method. The intercepts may contain the effect of space charging or the system error in the measurements, and thus can serve as a calibration to the measurements. The slopes are the major concern in the current decoding exercises since it depends on the surface treatment, particles size, and interaction between particle and substrate for substantiate particles.<sup>69</sup>

To elucidate the size effect on the CLS of Pt and Rh nanoclusters, we firstly calculated the dimensionality  $\tau$  and the bond nature indicator  $m$ . The  $E_v(0)$  and  $\Delta E_v(\infty)$  of the Pt-4*f*<sub>7/2</sub> can be obtained by applying Eqn (6) to Pt NPs deposited on pristine CNTs,<sup>64</sup> TiO<sub>2</sub>(110) surface at room temperature,<sup>65</sup> and multiwall carbon nanotubes (MCNTs) without pretreatment<sup>15</sup> with  $m=1.00$ . The reason for taking 1, a value holds for metallic solid, is that there is barely reaction between Pt NPs and substrates.<sup>70</sup> It is found that the atomic trapping energy and its bulk shift for Pt is about 67.21 eV and 3.28 eV, respectively.<sup>71</sup> According to Eqn. (9),  $C$  and  $E_v(\infty)$  can be extracted by linearization of the measured binding energies of Pt and Rh nanoclusters with respect to  $K^{-1}$ . Taking the obtained CLS values to the simulation iteration of the measured size-dependent  $E_v(K)$  for Pt on HOPG and MCNTs gives  $m=2.56$ , which adds the contribution from the interfacial reaction between Pt and substrates to the  $m=1.00$ .<sup>14, 15</sup> Similarly, for Rh NPs deposited on TiO<sub>2</sub>(110)-(1x1) surface,<sup>66</sup> Ar<sup>+</sup>-pretreated TiO<sub>2</sub>(110) surface,<sup>67</sup> and TiO<sub>2</sub>(110) surface at 300 K and 160 K,<sup>68</sup> it is found that the bond nature indicator  $m=1.00$  due to the weak interaction between Rh NPs and substrates. The Rh 3*d*<sub>5/2</sub> binding energy of an isolated Rh atom and its bulk shift equals to 302.163 eV and 4.37 eV, respectively.<sup>72</sup> Compared to their bulk counterparts, the experimental results of Au,<sup>73</sup> Cu,<sup>74</sup> Pt,<sup>62</sup> and Rh<sup>72</sup> nanoclusters revealed a positive CLS, which is mainly due to the shorter and stronger bonds between under-coordinated atoms. By adjusting the  $m$  values, our predications based on the BOLS correlation are in good agreement in trend with the experimental observations.

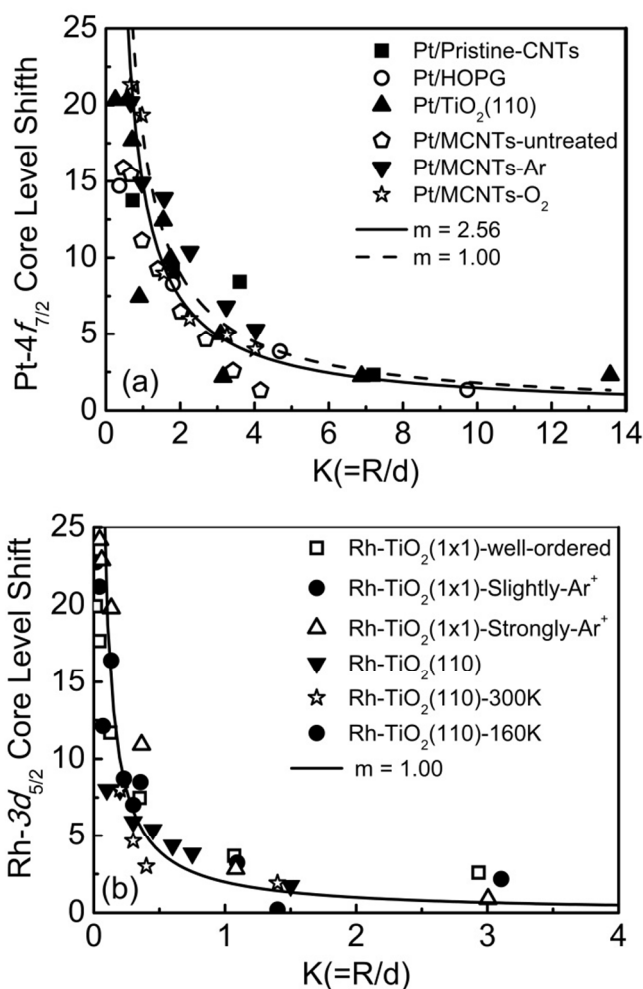


Fig.3. CLS predicted by the BOLS correlation (solid curve) and extracted from XPS measurements (scattered data) (a) Pt NPs deposited on pristine CNTs,<sup>64</sup> HOPG,<sup>14</sup> TiO<sub>2</sub>(110) at room temperature,<sup>65</sup> as well as Multi-wall CNTs-untreated and treated by Ar and O<sub>2</sub> plasma;<sup>15</sup> (b) Rh NPs deposited on the well-ordered, slightly Ar<sup>+</sup>-pretreated, and strongly Ar<sup>+</sup>-pretreated TiO<sub>2</sub>(110)-(1x1) surfaces,<sup>66</sup> TiO<sub>2</sub>(110) surface at 300K,<sup>67</sup> as well as TiO<sub>2</sub>(110) surface at 300 K and 160 K.<sup>68</sup>

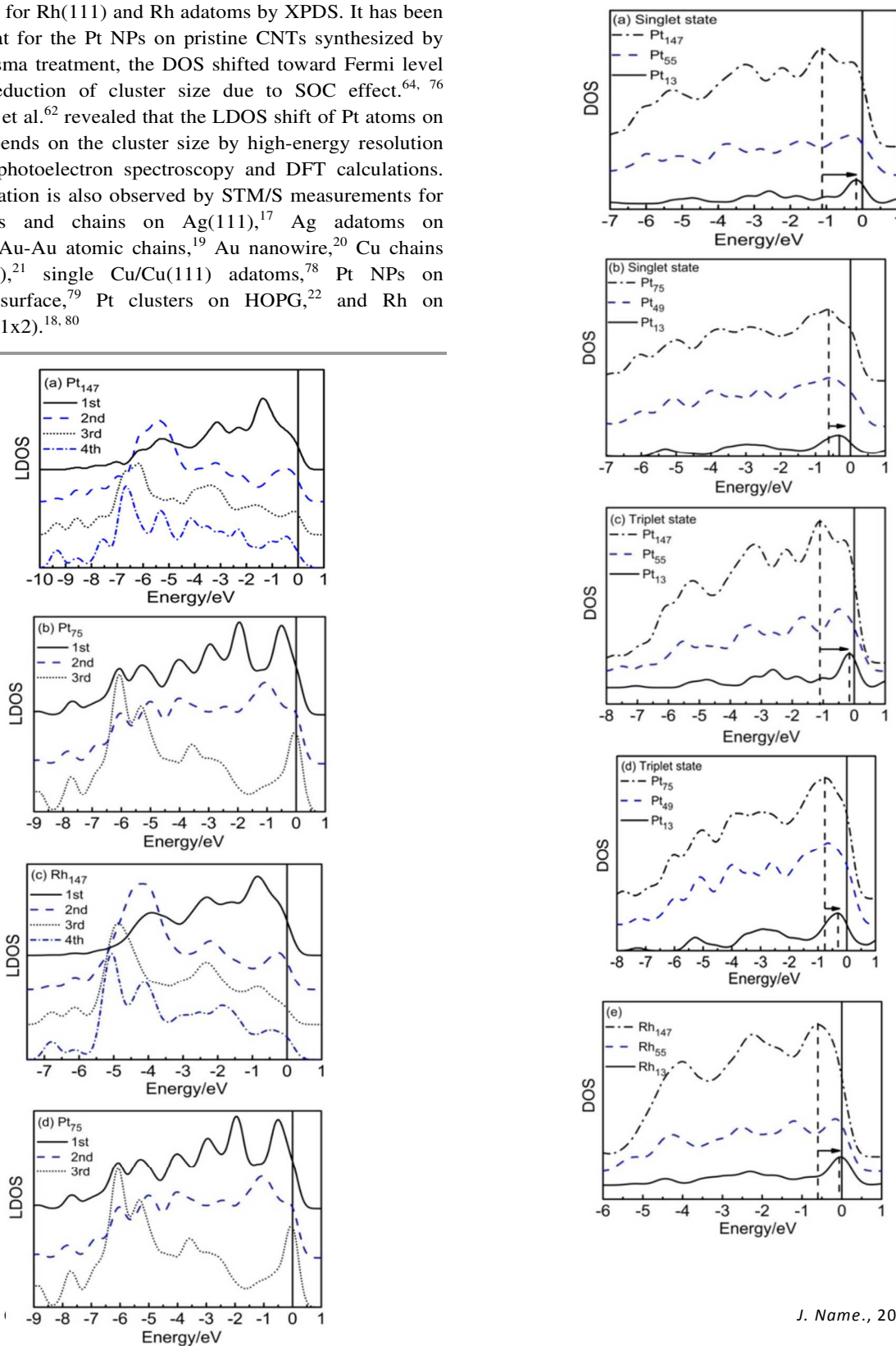
**Valence polarization.** According to the BOLS-NEP notation, the originally conductive *s*-electrons of Pt and Rh are expected to be polarized by the densely and tightly entrapped core charges. The magnitude of polarization increases as the electrons moves from the inner toward the edge with lower atomic CNs. This has been observed experimentally for Ag,<sup>17</sup> Au,<sup>19</sup> and Cu chains,<sup>21</sup> as well as for Pt<sup>18</sup> and Rh NPs.<sup>22</sup>

Fig. 4 plots the shell-resolved LDOS for 147-atom and 75-atom Pt and Rh nanoclusters. It is found that the valence electrons in the outermost shell shift toward  $E_f$ , whereas the entrapped electrons in the interior core remain at the lower edge. The maximum LDOS of atoms at the outermost shell are indeed polarized by the interior electrons. Therefore, the otherwise conducting electrons of the under-coordinated atoms become localized and polarized for Pt and Rh nanoclusters. Fig. 5 shows the extracted DOS, and indicates that the polarization becomes more significant for smaller NPs. The DOS peak shifts

from  $-0.59$  eV for  $\text{Rh}_{147}$  nanocluster to  $-0.07$  eV for  $\text{Rh}_{13}$  nanocluster in CO structures and from  $-0.78$  eV for  $\text{Pt}_{75}$  nanocluster to  $-0.34$  eV for  $\text{Pt}_{13}$  nanocluster in MD structures, demonstrating that the valence charge polarization is inversely proportional to the nanocluster size.

Moreover, the valence LDOS polarization of Pt and Rh nanoclusters is confirmed experimentally. For instance, Zheng et al.<sup>75</sup> observed the under-coordinated-induced valence polarization for Rh(111) and Rh adatoms by XPDS. It has been reported that for the Pt NPs on pristine CNTs synthesized by oxygen-plasma treatment, the DOS shifted toward Fermi level with the reduction of cluster size due to SOC effect.<sup>64, 76</sup> Bianchetti et al.<sup>62</sup> revealed that the LDOS shift of Pt atoms on Pt(111) depends on the cluster size by high-energy resolution core level photoelectron spectroscopy and DFT calculations. The polarization is also observed by STM/S measurements for Ag clusters and chains on Ag(111),<sup>17</sup> Ag adatoms on Ag(111),<sup>77</sup> Au-Au atomic chains,<sup>19</sup> Au nanowire,<sup>20</sup> Cu chains on Cu(111),<sup>21</sup> single Cu/Cu(111) adatoms,<sup>78</sup> Pt NPs on  $\text{TiO}_2(110)$  surface,<sup>79</sup> Pt clusters on HOPG,<sup>22</sup> and Rh on  $\text{TiO}_2(110)-(1 \times 2)$ .<sup>18, 80</sup>

**Fig.4.** Shell-resolved LDOS for (a) 147-atom Pt nanoclusters, (b) 75-atom Pt nanoclusters, (c) 147-atom Rh nanoclusters, and (d) 75-atom Rh nanoclusters. The outermost shell electrons move towards the upper edge near the Fermi level (allocated at 0 eV) while the interior shell remain at low energies for 5d-Pt and 4d-Rh.



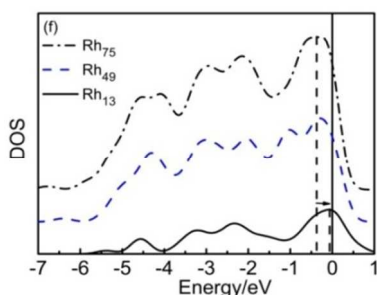
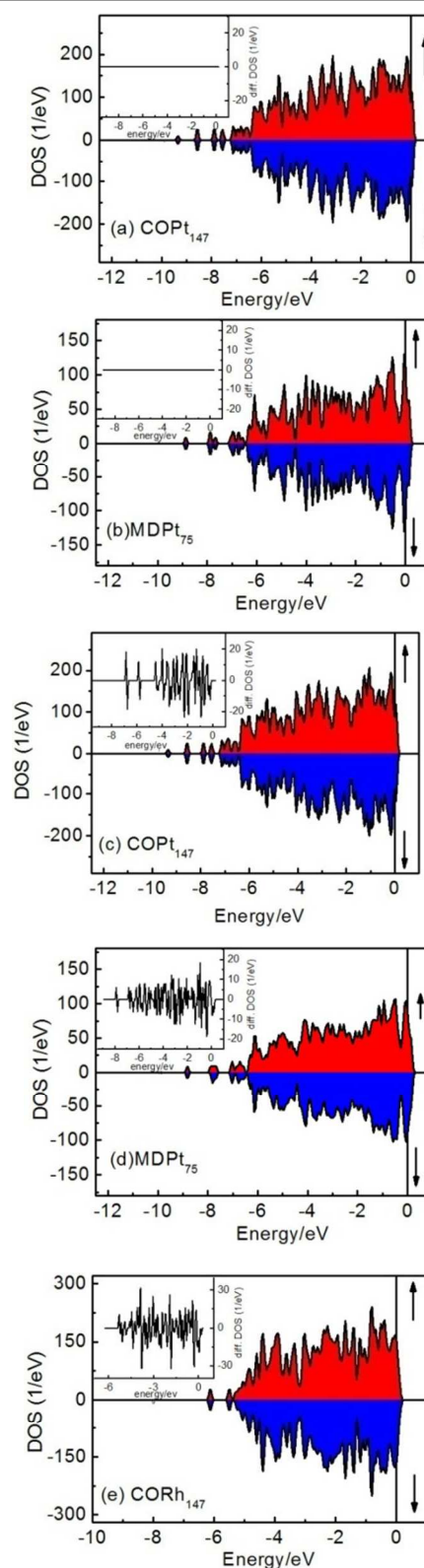


Fig. 5. Size-resolved DOS of (a, c, and e) CO structures and (b, d, and f) MD structures of  $Pt_N$  and  $Rh_N$  ( $N=13-147$  atoms) nanoclusters. The Fermi level is allocated at 0 eV.

**Localized magnetic moment.** The difference between the occupied majority and minority spin band is called magnetic moment, which is relative to the ferromagnetic exchange splitting between the bands.<sup>5</sup> As listed in Table 1, the magnetic moment of 147-atom CO structure of Rh NPs decreases from  $2.067 \mu$  in the outermost shell with CN = 3.4 to  $0.201 \mu$  in the interior core with CN = 12. Similar trend is observed for MD structures of Rh nanoclusters, and CO and MD structures of Pt nanoclusters, i.e., the magnetic moment value of nanoclusters increases with decreasing CN,<sup>81</sup> which are consistent with the previous results on Fe clusters<sup>82</sup> and Rh clusters.<sup>83, 84</sup>

**Magnetization.** Magnetic behaviour comes from spin-up ( $\alpha$ -spin states) and spin-down ( $\beta$ -spin states) states of metal  $d$ -band. The majority and minority spins of  $d$ -band is occupied by the spin-up electrons and unoccupied by the spin-down electrons that are located below and above of the Fermi energy level, respectively, depending on the magnetization direction of the atom. The positive and negative values represent the majority and minority spins, respectively. The Fermi level is allocated at 0 eV. In order to understand the origin of the magnetic behaviours of Pt and Rh nanoclusters, we calculated eigenvalue spectra by numerical integration of the DOS for spin-up and spin-down. To illustrate the mechanism of magnetization of Pt and Rh nanoclusters with different structures, Fig. 6 and Fig. 7 plot the spin-resolved DOS and partial DOS (PDOS) of Pt and Rh NPs consisting of 147 and 75 atoms, respectively. Detailed results on Pt and Rh nanoclusters of various sizes and structures are given in the supporting information. It is found that the DOS and PDOS distributions of spin-up and spin-down states split near Fermi level for triplet state of Pt NPs and quartet state of Rh NPs whereas no split is found for singlet state of Pt. Hence, the exchange correlation of electrons formed the ordered spin arrangement of electrons that determines the magnetic moment of these materials.



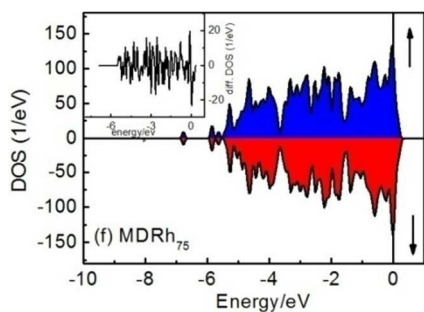


Fig.6. The spin-polarized DOS of (a and b) 5d-Pt singlet state, (c and d) 5d-Pt triplet state, and (e and f) 4d-Rh quartet state. Inset is the difference between spin-up and spin-down states in DOS. The spin-up and spin-down configurations are indicated by the up and down arrows, respectively. The Fermi level is set at 0 eV.

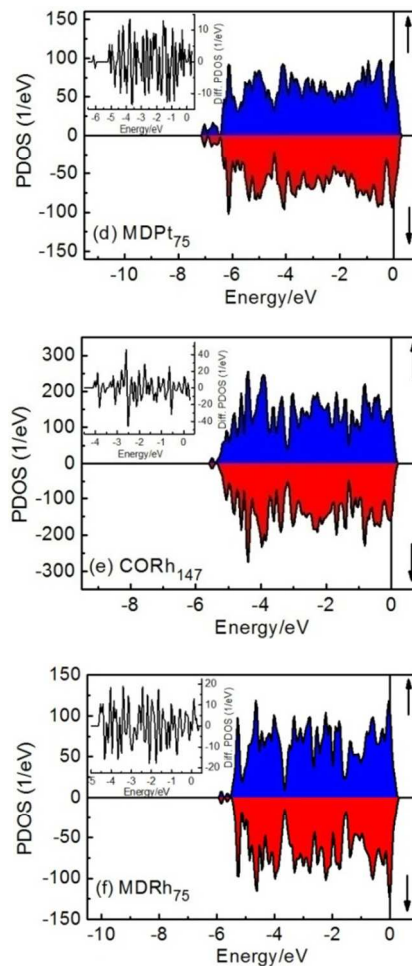
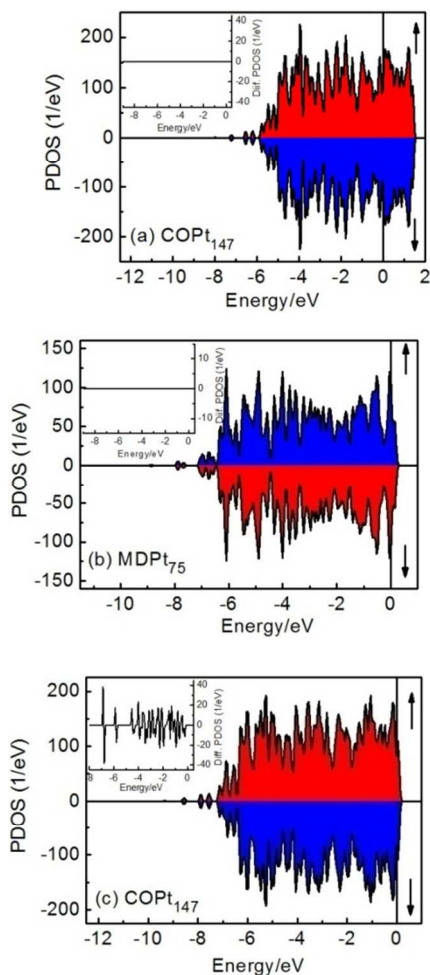


Fig.7. The spin-polarized PDOS of (a and b) 5d-Pt singlet state, (c and d) 5d-Pt triplet state, and (e and f) 4d-Rh quartet state. Inset is the difference between spin-up and spin-down states in PDOS. The spin-up and spin-down configurations are indicated by the up and down arrows, respectively. The Fermi level is set at 0 eV.

The energy gap of Pt and Rh nanoclusters between the highest occupied molecular orbital (HOMO) and the lowest unoccupied molecular orbital (LUMO) of  $\alpha$  and  $\beta$  spin states were calculated by DFT calculations, and the results are listed in Table 3. The anti-bonding and bonding are referred to as HOMO and LUMO. It is found that the gap between  $\alpha$  and  $\beta$  spin states of Pt (triplet state) and Rh (quartet state) increases as the number of atoms decreases for both CO and MD structures, whereas no gap is observed for Pt (singlet state). These findings confirmed that the magnetic properties are enhanced when the size of clusters decrease for Pt in triple state and Rh in quartet state because of the reduction of CN and the SOC effect.<sup>85</sup> The magnetic ordering is consistent with the previous theoretical calculations on Pd, Rh, and Ru nanoclusters,<sup>86</sup> Rh monolayers on Au,<sup>87</sup> Rh<sub>N</sub> and Pd<sub>N</sub> cluster up to N=13 atoms,<sup>88</sup> transition metal monolayers on noble metal(001) substrates,<sup>89</sup> Pt<sub>N</sub> (N=2-55 atoms) clusters,<sup>6</sup> Pt<sub>13</sub> clusters in a NaY zeolite,<sup>45</sup> Tc, Ru, Rh, and Pd monolayers on Ag(001) surface,<sup>90</sup> as well as Rh<sub>N</sub> clusters (N= 9, 13, 15, 17, and 19 atoms).<sup>44</sup> This is also confirmed by experimental observations of Pt embedded in a

polymer prepared by chemical reaction method,<sup>91</sup> Pt clusters by ion exchange of a KL zeolite,<sup>92</sup> Pt/Y<sub>3</sub>Fe<sub>5</sub>O<sub>12</sub> bilayers by X-ray magnetic circular dichroism (XMCD),<sup>93</sup> Pt nanoparticles induced by surface chemisorption,<sup>94</sup> Rh<sub>N</sub> (N=12-32 atoms) grown by laser vaporization,<sup>2</sup> Rh monolayers deposited by grown layer method on Fe,<sup>95</sup> as well as Rh NPs prepared by reducing cation in solution.<sup>3</sup> No magnetic behaviour is reported for Pt clusters with 13-20 atoms in zeolite Y<sup>96</sup> and Pt clusters on graphene<sup>97</sup> that are consistent with our theoretical calculation for Pt in singlet state. Consequently, the HOMO-LUMO gap and the magnetic behaviour of Pt nanoclusters in triplet state and Rh nanoclusters in quartet state clusters are related the cluster size.

**Table 3.** The calculated gaps for spin-up ( $\alpha$ ) and spin-down ( $\beta$ ) of Pt nanoclusters in singlet and triplet states and Rh nanoclusters in quartet state. The magnetism behaviour of 4d and 5d clusters occurs in the triplet of Pt and quartet of Rh.

	Gap Up-Spin alpha (eV)			Gap Down-Spin Beta (eV)		
	Pt Singlet	Pt Triplet	Rh	Pt Singlet	Pt Triplet	Rh
CO <sub>13</sub>	1.009	0.058	0.976	1.009	1.005	0.982
CO <sub>55</sub>	0.305	0.252	0.092	0.305	0.253	0.055
CO <sub>147</sub>	0.274	0.063	0.013	0.274	0.091	0.034
MD <sub>13</sub>	0.417	0.224	0.334	0.417	0.416	0.105
MD <sub>49</sub>	0.374	0.363	0.068	0.374	0.361	0.022
MD <sub>75</sub>	0.236	0.187	0.028	0.236	0.054	0.052

## Conclusions

Consistency in trend between DFT calculations and experimental observations such as EXAFS, STM/S, XPDS, and XPS measurements confirmed our predications based on BOLS-NEP correlation that the under-coordination affects the properties of Pt and Rh nanoclusters including the bond relaxation, lattice strain, charge transfer, core electron entrapment, valence electron polarization, and magnetic moment. The atomic under-coordination induces local bond contraction, densification and entrapment of core electrons, valence charge polarization as well as magnetization, giving rise to the unusual properties of Pt and Rh nanoclusters in terms of the size dependence and the emergence of new properties, which are lack in their parent bulk materials. The results of this work will contribute to the understanding of the intriguing properties of Pt and Rh nanoclusters such as catalytic enhancement and magnetization.

## Notes and references

<sup>a</sup>NOVITAS, School of Electrical and Electronic Engineering, Nanyang Technological University, 639798 Singapore, ecqsun@ntu.edu.sg.

<sup>b</sup>Center for Coordination Bond Engineering, School of Materials Science and Engineering, China Jiliang University, Hangzhou 310018, China, ygong2007@gmail.com.

†Electronic Supplementary Information (ESI) available: [details of any supplementary information available should be included here]. See DOI: 10.1039/b000000x/

- C. Q. Sun, *Relaxation of the Chemical Bond*, Springer Series in Chemical Physics, 2014.
- A. J. Cox, J. G. Louderback and L. A. Bloomfield, *Phys. Rev. Lett.*, 1993, **71**, 923-926.
- Y. T. Jeon and G. H. Lee, *J. Appl. Phys.*, 2008, **103**, 094313-094315.
- X. Liu, M. Bauer, H. Bertagnolli, E. Roduner, J. van Slageren and F. Phillipp, *Phys. Rev. Lett.*, 2006, **97**, 253401-253404.
- D. Sellmyer and S. Ralph, *Advanced magnetic nanostructures*, Springer, New York, 2006.
- L. Xiao and L. Wang, *J. Phys. Chem. A*, 2004, **108**, 8605-8614.
- Y. Liu and W. E. Mustain, *ACS Catalysis*, 2011, **1**, 212-220.
- E. Roduner, *Chem. Soc. Rev.*, 2006, **35**, 583-592.
- F. Porrati, R. Sachser and M. Huth, *J. Phys.: Condens. Matter*, 2014, **26**, 085302-085308.
- T. Imaoka, H. Kitazawa, W.-J. Chun, S. Omura, K. Albrecht and K. Yamamoto, *J. Am. Chem. Soc.*, 2013, **135**, 13089-13095.
- S. H. Lee, S. S. Han, J. K. Kang, J. H. Ryu and H. M. Lee, *Surf. Sci.*, 2008, **602**, 1433-1439.
- G. Rupprechter, K. Hayek and H. Hofmeister, *Vacuum*, 1995, **46**, 1035-1040.
- A. Renou and M. Gillet, *Surf. Sci.*, 1981, **106**, 27-34.
- P. Marcus and C. Hinnen, *Surf. Sci.*, 1997, **392**, 134-142.
- D.-Q. Yang and E. Sacher, *J. Phys. Chem. C*, 2008, **112**, 4075-4082.
- D.-Q. Yang and E. Sacher, *Chem. Mater.*, 2006, **18**, 1811-1816.
- A. Sperl, J. Kröger, N. Néel, H. Jensen, R. Berndt, A. Franke and E. Pehlke, *Phys. Rev. B*, 2008, **77**, 085422-085428.
- A. Berkó and F. Solymosi, *Surf. Sci.*, 1998, **400**, 281-289.
- J. N. Crain and D. T. Pierce, *Science*, 2005, **307**, 703-706.
- K. Schouteden, E. Lijnen, D. A. Muzychenko, A. Ceulemans, F. C. Liviu, P. Lievens and C. V. Haesendonck, *Nanotechnology*, 2009, **20**, 395401-395408.
- S. Fölsch, P. Hyldgaard, R. Koch and K. H. Ploog, *Phys. Rev. Lett.*, 2004, **92**, 056803-056806.
- U. Müller, K. Sattler, J. Xhie, N. Venkateswaran and G. Raina, *J. Vac. Sci. Technol. B*, 1991, **9**, 829-832.
- S. Duan, P.-P. Fang, F.-R. Fan, I. Broadwell, F.-Z. Yang, D.-Y. Wu, B. Ren, C. Amatore, Y. Luo, X. Xu and Z.-Q. Tian, *Phys. Chem. Chem. Phys.*, 2011, **13**, 5441-5449.
- J. C. Davis, M. Bühl and K. R. Koch, *J. Phys. Chem. A*, 2013, **117**, 8054-8064.
- X. Zhang, J.-I. Kuo, M. Gu, X. Fan, P. Bai, Q.-G. Song and C. Q. Sun, *Nanoscale*, 2010, **2**, 412-417.
- S. Ahmadi, X. Zhang, Y. Gong, C. H. Chia and C. Q. Sun, *Phys. Chem. Chem. Phys.*, 2014, **16**, 8940-8948.
- M. A. Omar, *Elementary solid state physics: principles and applications*, Addison-Wesley, New York, Reading, Mass., 1993.
- V. M. Goldschmidt, *Berichte der deutschen chemischen Gesellschaft (A and B Series)*, 1927, **60**, 1263-1296.
- L. Pauling, *J. Am. Chem. Soc.*, 1947, **69**, 542-553.
- W. J. Huang, R. Sun, J. Tao, L. D. Menard, R. G. Nuzzo and J. M. Zuo, *Nat. Mater.*, 2008, **7**, 308-313.
- G. Rupprechter, K. Hayek and H. Hofmeister, *Nanostruct. Mater.*, 1997, **9**, 311-314.
- C. Kim and H. Lee, *Catal. Commun.*, 2009, **11**, 7-10.
- T. Fukushima, K. Matshzawa, H. Yamada, A. Tasaka and M. Inaba, *ECS Meeting Abstracts*, 2008, **MA2008-02**, 913.
- S. Dobrin, *Phys. Chem. Chem. Phys.*, 2012, **14**, 12122-12129.
- A. V. Myshlyavtsev and P. V. Stishenko, *Adsor*, 2013, **19**, 795-801.
- G. Rupprechter, K. Hayek and H. Hofmeister, *J. Catal.*, 1998, **173**, 409-422.
- N. Watari and S. Ohnishi, *Phys. Rev. B*, 1998, **58**, 1665-1677.
- B. Piveteau, M.-C. Desjonquères, A. M. Oles and D. Spanjaard, *Phys. Rev. B*, 1996, **53**, 9251-9266.
- B. Delley, *J. Chem. Phys.*, 1990, **92**, 508-517.

40. B. Delley, *J. Phys.: Condens. Matter*, 2010, **22**, 384208-384213.
41. B. Delley, *Phys. Rev. B*, 2002, **66**, 155125-155133.
42. J. P. Perdew and Y. Wang, *Phys. Rev. B*, 1992, **45**, 13244-13249.
43. R. H. M. Smit, C. Untiedt, A. I. Yanson and J. M. van Ruitenbeek, *Phys. Rev. Lett.*, 2001, **87**, 266102-266105.
44. S. R. Bahn and K. W. Jacobsen, *Phys. Rev. Lett.*, 2001, **87**, 266101-266104.
45. J. Bartolomé, F. Bartolomé, L. M. García, E. Roduner, Y. Akdogan, F. Wilhelm and A. Rogalev, *Phys. Rev. B*, 2009, **80**, 014404-014413.
46. H. Y. Sang, A. D. David, B. A. James, O. Pablo and G. Keith, *J. Phys.: Condens. Matter*, 1997, **9**, L39-L45.
47. K. Balasubramanian, *J. Chem. Phys.*, 1987, **87**, 6573-6578.
48. L. Zhi-Qiang, Y. Jing-Zhi, K. Ohno and Y. Kawazoe, *J. Phys.: Condens. Matter*, 1995, **7**, 47-53.
49. Y. Jinlong, F. Toigo and W. Kelin, *Phys. Rev. B*, 1994, **50**, 7915-7924.
50. P. Villaseñor-González, J. Dorantes-Dávila, H. Dreyssé and G. M. Pastor, *Phys. Rev. B*, 1997, **55**, 15084-15091.
51. C. Barreateau, M. C. Desjonquères and D. Spanjaard, *Eur. Phys. J. D*, 2000, **11**, 395-402.
52. M. Klimentov, S. Nepijko, H. Kühlenbeck, M. Bäumer, R. Schlögl and H. J. Freund, *Surf. Sci.*, 1997, **391**, 27-36.
53. Y. G. Shen, D. J. O'Connor and R. J. MacDonald, *Nuclear Instruments and Methods in Physics Research Section B: Beam Interactions with Materials and Atoms*, 1998, **135**, 361-365.
54. C. Solliard and M. Flueli, *Surf. Sci.*, 1985, **156**, Part 1, 487-494.
55. J. L. Fulton, J. C. Linehan, T. Autrey, M. Balasubramanian, Y. Chen and N. K. Szymczak, *J. Am. Chem. Soc.*, 2007, **129**, 11936-11949.
56. C. Q. Sun, *Phys. Rev. B*, 2004, **69**, 045105-045112.
57. M. D. Segall, *Mol. Phys.*, 1996, **89**, 571-577.
58. A. Moghaddasi, M. Zahedi and P. Watson, *J. Phys. Chem. C*, 2012, **116**, 5014-5018.
59. C. J. Heard and R. L. Johnston, *Eur. Phys. J. D*, 2013, **67**, 1-6.
60. R. L. J. Fuyi Chen, *Acta Mater.*, 2008, **56**, 2374-2380.
61. M. Zaccagna, C. Astaldi, K. C. Prince, M. Sastry, C. Comicioli, R. Rosei, C. Quaresima, C. Ottaviani, C. Crotti, A. Antonini, M. Matteucci and P. Perfetti, *Surf. Sci.*, 1996, **347**, 53-62.
62. L. Bianchettin, A. Baraldi, S. de Gironcoli, E. Vesselli, S. Lizzit, L. Petaccia, G. Comelli and R. Rosei, *J. Chem. Phys.*, 2008, **128**, 114706-114711.
63. A. Baraldi, L. Bianchettin, E. Vesselli, S. de Gironcoli, S. Lizzit, L. Petaccia, G. Zampieri, G. Comelli and R. Rosei, *New J. Phys.*, 2007, **9**, 143-154.
64. C. Bittencourt, M. Hecq, A. Felten, J. J. Pireaux, J. Ghijsen, M. P. Felicissimo, P. Rudolf, W. Drube, X. Ke and G. Van Tendeloo, *Chem. Phys. Lett.*, 2008, **462**, 260-264.
65. H.-P. Steinrück, F. Pesty, L. Zhang and T. E. Madey, *Phys. Rev. B*, 1995, **51**, 2427-2439.
66. A. Berkó, I. Ulrych and K. C. Prince, *J. Phys. Chem. B*, 1998, **102**, 3379-3386.
67. H. R. Sadeghi and V. E. Henrich, *Appl. Surf. Sci.*, 1984, **19**, 330-340.
68. L. Óvári and J. Kiss, *Appl. Surf. Sci.*, 2006, **252**, 8624-8629.
69. C. Q. Sun, L. K. Pan, H. L. Bai, Z. Q. Li, P. Wu and E. Y. Jiang, *Acta Mater.*, 2003, **51**, 4631-4636.
70. C. Q. Sun, B. K. Tay, X. T. Zeng, S. Li, T. P. Chen, Z. Ji, H. L. Bai and E. Y. Jiang, *J. Phys.: Condens. Matter*, 2002, **14**, 7781-7795.
71. C. Q. Sun, Y. Wang, Y. Nie, Y. Sun, J. Pan, L. Pan and Z. Sun, *J. Phys. Chem. C*, 2009, **113**, 21889-21894.
72. Y. Wang, Y. G. Nie, J. S. Pan, L. K. Pan, Z. Sun, L. L. Wang and C. Q. Sun, *Phys. Chem. Chem. Phys.*, 2010, **12**, 2177-2182.
73. T. Ohgi and D. Fujita, *Phys. Rev. B*, 2002, **66**, 115410-115415.
74. D. Q. Yang and E. Sacher, *Appl. Surf. Sci.*, 2002, **195**, 187-195.
75. W. Zheng, J. Zhou and C. Q. Sun, *Phys. Chem. Chem. Phys.*, 2010, **12**, 12494-12498.
76. K. A. Mills, R. F. Davis, S. D. Kevan, G. Thornton and D. A. Shirley, *Phys. Rev. B*, 1980, **22**, 581-592.
77. A. Sperl, J. Kröger, R. Berndt, A. Franke and E. Pehlke, *New J. Phys.*, 2009, **11**, 063020-063027.
78. J. Lagoute, X. Liu and S. Fölsch, *Phys. Rev. Lett.*, 2005, **95**, 136801-1368014.
79. J. Szőko and A. Berkó, *Vacuum*, 2003, **71**, 193-199.
80. A. Berkó, G. Ménesi and F. Solymosi, *Surf. Sci.*, 1997, **372**, 202-210.
81. P. J. Jensen and K. H. Bennemann, *Z. Phys. D*, 1995, **35**, 273-278.
82. F. Aguilera-Granja, J. M. Montejano-Carrizales and J. L. Morán-López, *Phys. Lett. A*, 1998, **242**, 255-260.
83. H. Sun, Y. Ren, Y.-H. Luo and G. Wang, *Physica B: Condens. Matter*, 2001, **293**, 260-267.
84. E. O. Berlanga-Ramírez, F. Aguilera-Granja, A. Díaz-Ortiz, J. L. Rodríguez-López and A. Vega, *Phys. Lett. A*, 2003, **318**, 473-479.
85. S. N. Khanna, F. Cyrot-Lackmann, Y. Boudeville and J. Rousseau-Voilet, *Surf. Sci.*, 1981, **106**, 287-292.
86. B. V. Reddy, S. N. Khanna and B. I. Dunlap, *Phys. Rev. Lett.*, 1993, **70**, 3323-3326.
87. M. J. Zhu, D. M. Bylander and L. Kleinman, *Phys. Rev. B*, 1991, **43**, 4007-4010.
88. T. Futschek, M. Marsman and J. Hafner, *J. Phys.: Condens. Matter*, 2005, **17**, 5927-5963.
89. S. Blügel, *Phys. Rev. Lett.*, 1992, **68**, 851-854.
90. O. Eriksson, R. C. Albers and A. M. Boring, *Phys. Rev. Lett.*, 1991, **66**, 1350-1353.
91. Y. Yamamoto, T. Miura, Y. Nakae, T. Teranishi, M. Miyake and H. Hori, *Physica B: Condens. Matter*, 2003, **329-333**, Part 2, 1183-1184.
92. C. Jensen, J. van Slageren, P. Jakes, R.-A. Eichel and E. Roduner, *J. Phys. Chem. C*, 2013, **117**, 22732-22745.
93. S. Geprägs, S. Meyer, S. Altmannshofer, M. Opel, F. Wilhelm, A. Rogalev, R. Gross and S. T. B. Goennenwein, *Appl. Phys. Lett.*, 2012, **101**, 262407-262410.
94. Y. Sakamoto, Y. Oba, H. Maki, M. Suda, Y. Einaga, T. Sato, M. Mizumaki, N. Kawamura and M. Suzuki, *Phys. Rev. B*, 2011, **83**, 104420-104432.
95. T. Kachel, W. Gudat, C. Carbone, E. Vescovo, S. Blügel, U. Alkemper and W. Eberhardt, *Phys. Rev. B*, 1992, **46**, 12888-12891.
96. J. de Graaf, A. J. van Dillen, K. P. de Jong and D. C. Koningsberger, *J. Catal.*, 2001, **203**, 307-321.
97. H. D. Ozaydin, H. Sahin, R. T. Senger and F. M. Peeters, *Ann. Phys.*, 2014, **1-7**, 1-7.